



# An upper limit to the sodium layer longitudinal and transversal altitude structure function from MCAO data

F. Rigaut<sup>1</sup>\* and B. Neichel<sup>2</sup>

<sup>1</sup>Research School of Astronomy & Astrophysics, Australian National University, Mount Stromlo Observatory, Cotter Road, Weston Creek, ACT 2611, Australia

<sup>2</sup>Gemini Observatory, c/o AURA, Casilla 603 La Serena, Chile

Accepted 2013 February 23. Received 2013 February 10

## ABSTRACT

The Gemini Multi-Conjugate Adaptive Optics System is the first sodium-based Multi-Laser Guide Star (LGS) Adaptive Optics system used for astronomy. It uses five LGSs distributed on a 1 arcmin<sup>2</sup> constellation to measure and compensate for atmospheric distortions. In this Letter, we use the LGS wavefront sensor data to derive the amount of differential focus caused by horizontal sodium layer structures, which we call the focus excess (because it comes in addition to the turbulent part). Based on data accumulated at a rate of around 1 week per month during a period of 1 year, we derive an upper limit of the focus excess of  $15 \pm 60$  nm rms for an 8-m telescope over an 85 arcsec baseline. No anisotropy in the spatial distribution of this error is detected.

**Key words:** atmospheric effects – instrumentation: adaptive optics – site testing – telescopes.

## 1 INTRODUCTION

Adaptive optics (AO) is a technique that aims at compensating quickly varying optical aberrations to restore the ultimate angular resolution limit of an optical system. It uses a combination of wavefront sensors (WFSs), to analyse the light-wave aberrations, and deformable mirrors (DMs), to compensate them. Astronomical observations with AO can only be obtained in the vicinity of relatively bright stars ( $R \sim 15$ ). This puts a severe restriction on performance, limiting the fraction of the sky accessible to only about 5 per cent. This realization led to the idea of using laser guide stars (LGSs) to create bright artificial stars that could be used for AO compensation at any position in the sky (Foy & Labeyrie 1985). A so-called ‘sodium LGS’ can be created from resonant backscattering of sodium atoms in a mesospheric layer that lies between 90 and 100 km above sea level. Today, most of the largest ground-based telescopes are equipped with such lasers (Amico, Campbell & Christou 2010). Recently, the Gemini Observatory produced the first sodium LGS constellation to feed a Multi-Conjugate Adaptive Optics (MCAO) system at the Gemini South 8-m telescope (d’Orgeville et al. 2012; Rigaut et al. 2012), located at Cerro Pachón, Chile (latitude 30°25 South). The Gemini MCAO System, called GeMS, uses five LGSs feeding an equal number of  $16 \times 16$  subaperture LGS Shack–Hartmann WFSs to measure atmospheric distortions. Compensation is done by two DMs conjugated optically at 0 and 9 km above site and totalling 320 actuators.

The performance of a LGS AO system varies with the sodium layer structure and dynamics. For instance, a good knowledge of

the sodium abundance is crucial to understand the fluctuations of the LGS brightness during the year (Moussaoui et al. 2010; Neichel et al. 2013). The sodium layer *thickness*, through a simple parallax effect, impacts the signal-to-noise ratio of the subapertures located farthest from the laser launch location (Lardiere et al. 2010; Muller et al. 2010). Fluctuations of the *mean sodium altitude* (changes of the vertical structure of the sodium layer) lead to focus drift and thus bias the measurement of the atmospheric turbulence focus (Pfrommer, Hickson & Chiao-Yao 2010; Pfrommer & Hickson 2010, 2012b).

For AO systems using multiple LGSs,<sup>1</sup> the differential mean sodium altitude between LGSs is also of importance as it can possibly lead to significant loss in performance. Multi-LGS AO systems typically perform a tomographic reconstruction of the atmospheric turbulence volume above the telescope, using the signal from all the WFSs. A differential mean sodium altitude leads to a differential focus error in each sensing direction, which will be ‘aliased’ through the tomographic reconstruction into high-order, field-varying aberrations. This is a key parameter for the performance of GeMS, but even more so for Extremely Large Telescope (ELT) LGS AO systems, given that this effect scales with the square of the telescope diameter.

Pfrommer & Hickson (2012a) present results obtained at the University of British Columbia Large Zenith Telescope Lidar on the structure function of the sodium layer average altitude versus longitudinal and transversal angles with respect to the wind

<sup>1</sup> To date, and of particular relevance, all planned ELT LGS AO systems are designed to use multiple LGSs in order to reduce the cone effect (Tallon & Foy 1990).

\*E-mail: francois.rigaut@anu.edu.au

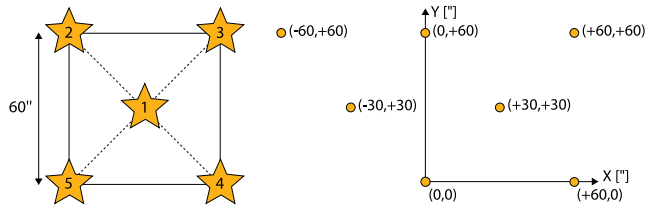


**Figure 1.** Left-hand panel: GeMS LGS constellation geometry on the sky. The five beams are sent in a constellation with four LGSs at the corner of a 60 arcsec square, plus one in the centre. The number assigned to each LGS follows the LGS WFS numbering system used in this Letter. Right-hand panel: baselines spanned by all LGS pairs. Note that by definition of the structure function,  $D(x, y) = D(-x, -y)$ , so that only half of the points/baselines are drawn here.

direction. These results show a large anisotropy: in the transversal direction (i.e. perpendicular to the wind direction), the sodium layer altitude varies much more (and/or much more rapidly) than in the longitudinal direction (i.e. parallel to the wind direction). According to their results, for a 39-m-diameter telescope and for a 30-m horizontal separation between LGSs at the sodium layer altitude, one should expect about  $0.8 \mu\text{m}$  of rms differential focus error for a separation vector parallel to the wind direction, and  $7 \mu\text{m}$  for a vector perpendicular to the wind direction. For the Gemini 8-m telescope, noting that this effect scales as  $D^2$ , this would translate into a differential focus rms error of 30 nm (parallel) and 280 nm (perpendicular).

The GeMS constellation is made of four LGSs distributed over a square of size 60 arcsec (or 26 m at the 90-km-high sodium layer when observing at zenith), plus a fifth LGS at its centre (see Fig. 1). This provides an ideal setup and geometry to investigate the effect described by Pfrommer & Hickson (2012a), with six different baselines ranging from 42 to 85 arcsec, and covering four different position angles (orientation on the sky).

In this Letter, we carry an analysis of the GeMS LGS WFS data to derive the amount of differential focus (i.e. the difference of focus between two pointing separated by  $\theta_0$ ) in excess to what is expected from turbulence. Throughout this letter, that additional contribution is called *focus excess*. It is expressed in nanometres (rms). The mathematical expression of the focus excess is derived in the next section.

Taking advantage of the GeMS LGS constellation geometry, we investigate any potential anisotropy in the focus excess. Section 2 exposes the method and data processing and Section 3 presents the results and discussion. Familiarity with the subject, for instance, by having read Pfrommer & Hickson (2012a) will facilitate the understanding of the current letter.

## 2 METHOD AND DATA PROCESSING

The focus induced by sodium layer altitude variations is uncorrelated with the atmospheric turbulence focus. As a result, both will thus combine quadratically. Similarly, the angular *differential* focus, that is, the differential focus between two directions separated by a given angle  $\theta_0$ , is the Root Sum of Squares (RSS) contribution of the differential atmospheric turbulent focus and the sodium layer altitude-induced differential focus.

Noting  $m_n$ ,  $a_n$  and  $h_n$  the measured, turbulent and sodium layer altitude components for Zernike mode  $n$  [in this Letter, we follow Noll (1976) notation, i.e. 4 is the focus, and 5 and 6 are the two

astigmatisms; note that  $h_n = 0$  for  $n \neq 4$ ] we have, neglecting the noise,

$$m_4 = a_4 + h_4. \quad (1)$$

Let us also introduce the shorthand notation [where the bold italic symbols are vectors, e.g.  $\theta = (\theta_x, \theta_y)$ ]

$$\delta f(\theta, \theta_0) = f(\theta + \theta_0) - f(\theta), \quad (2)$$

where  $f$  is generic and can be replaced by  $m$ ,  $a$  or  $h$ .

In this study, we use the fact that the angular differential atmospheric turbulent focus can be estimated from the differential astigmatism. Noll (1976) demonstrated that, for a circular non-obstructed aperture, the single-direction variance of the coefficients of focus and astigmatism modes induced by atmospheric turbulence is the same, that is,

$$\langle a_4^2 \rangle = \langle a_5^2 \rangle = \langle a_6^2 \rangle, \quad (3)$$

where  $\langle \rangle$  denotes an ensemble average over time.

From Roddier et al. (1993), we find that, for any angle  $\theta$ , the angular correlation function of the focus is equal to the average of the angular correlation functions of the two astigmatism.

$$C_{44}(\theta) = \frac{1}{2} [C_{55}(\theta) + C_{66}(\theta)]. \quad (4)$$

Combining these two results, it is easy to show that the differential turbulent focus between two arbitrary directions should be equal to the average of the differential astigmatism:

$$\begin{aligned} \langle \delta a_4^2(\theta_0) \rangle &= \langle (a_4(\theta + \theta_0) - a_4(\theta))^2 \rangle \\ &= 2 \langle a_4^2 \rangle (1 - C_{44}(\theta_0)) \\ &= \langle a_5^2 \rangle (1 - C_{55}(\theta_0)) + \langle a_6^2 \rangle (1 - C_{66}(\theta_0)) \\ &= \frac{1}{2} [\langle \delta a_5^2(\theta_0) \rangle + \langle \delta a_6^2(\theta_0) \rangle]. \end{aligned} \quad (5)$$

Now let us express  $\sigma_{\delta h_4}^2$ , the variance of the focus excess. From equation (1), we have

$$\langle \delta m_4^2(\theta_0) \rangle = \langle \delta a_4^2(\theta_0) \rangle + \langle \delta h_4^2(\theta_0) \rangle$$

as turbulence and sodium layer altitude effects ought to be uncorrelated. Using equation (5)

$$\begin{aligned} \langle \delta h_4^2(\theta_0) \rangle &= \langle \delta m_4^2(\theta_0) \rangle \\ &\quad - \frac{1}{2} [\langle \delta a_5^2(\theta_0) \rangle + \langle \delta a_6^2(\theta_0) \rangle] \end{aligned}$$

and finally

$$\begin{aligned} \sigma_{\delta h_4}^2(\theta_0) &= \langle \delta h_4^2(\theta_0) \rangle = \langle \delta m_4^2(\theta_0) \rangle \\ &\quad - \frac{1}{2} [\langle \delta m_5^2(\theta_0) \rangle + \langle \delta m_6^2(\theta_0) \rangle] \end{aligned} \quad (6)$$

which is simply saying that the variance of the focus excess  $\sigma_{\delta h_4}^2$  is equal to the difference of the variance of the measured differential focus with the average variance of the measured differential astigmatism, both available readily from the GeMS LGS WFS data. Using these data,  $\sigma_{\delta h_4}^2(\theta_0)$  can be computed for each of the six LGS WFS baselines.

One issue with equation (6) is that, because of noise and other error sources, it is possible for  $\sigma_{\delta h_4}^2(\theta_0)$  to be negative. For the final expression of the focus excess (in nm rms), we propose to use the following:

$$\sigma_{\delta h_4}(\theta_0) = \text{sign}(\sigma_{\delta h_4}^2(\theta_0)) |\sigma_{\delta h_4}^2(\theta_0)|^{1/2}. \quad (7)$$

The raw data collected from GeMS are of two types. In the first type, data saved directly from the real-time computer are called circular buffers (CBs). CBs contain LGS WFS slopes and DM actuator commands for up to 24 000 contiguous AO loop frames, which corresponds to 120 s for a 200-Hz GeMS main loop rate.<sup>2</sup> The second type, called Real-Time Display (RTD) buffers, is saved from the telemetry system and contains basically the same data, but sampled only at 40 Hz approximately, irrespective of the AO loop rate. These files are 5000 samples long, covering about 2 min. The RTD buffers can be saved continuously, providing nearly seamless coverage of arbitrarily large fractions of the nights.

The method used in this Letter is based on a modal open-loop (OL) statistical analysis. OL measurements are reconstructed from the LGS WFS closed-loop residual slopes and added to the DM commands, properly time-registered and projected in the WFS space using the system interaction matrix. Slopes are then projected on the first 45 Zernike modes. Zernike modes were selected because their statistical properties are well known for Kolmogorov and von Karman turbulence. At the end of this process, time series of 45 Zernike coefficients are available for the five LGS WFSs. From these data, the following quantities can be computed:

- (i) Coefficient variances per WFS.
- (ii) Variance of the differential coefficients, i.e. variance of the difference of the coefficient time series from two WFSs.
- (iii) Power spectral densities (PSDs) of the coefficient time series and the differential coefficient time series.

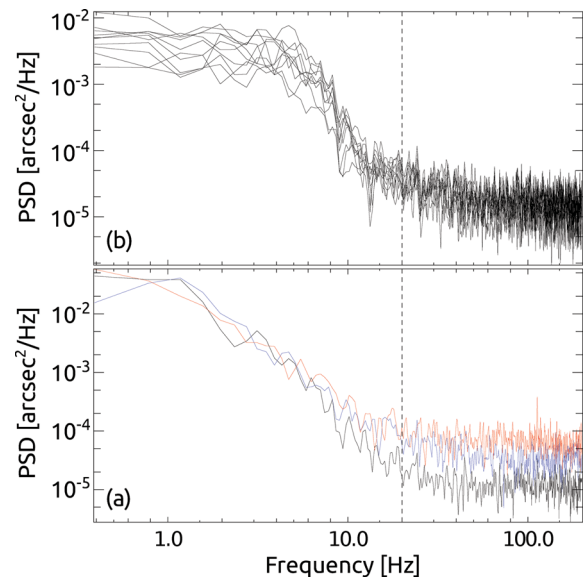
A last step is to remove the noise contribution from the computed variances and differential coefficient variances. The noise on each Zernike coefficient time series is estimated using the high-frequency part of the coefficient PSDs. The cut-off frequency is adjusted for each CB, and typically chosen to be one-tenth of the sampling frequency. Fig. 2(a) shows an example of a PSD obtained for a CB acquired in the night of 2012 January 8, for the focus (black) and the two astigmatism modes (blue and red). The vertical dashed line shows the frequency cut-off for noise estimation. These estimated noise values are then used to unbias the Zernike coefficient variances and differential variances.

### 3 RESULTS AND DISCUSSION

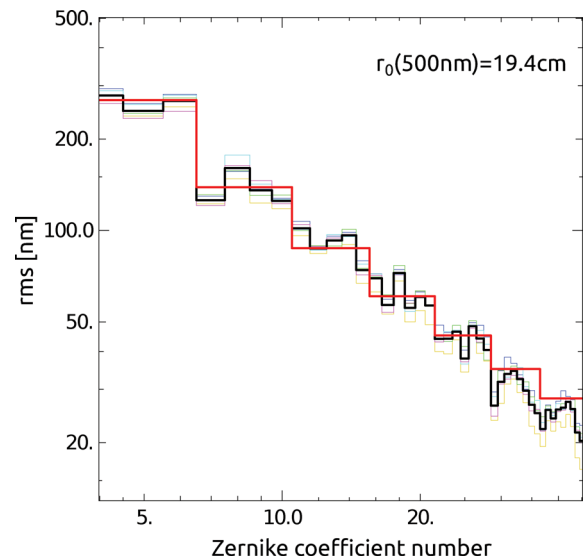
Fig. 3 shows an example of the canonical Zernike coefficient variance plot, the fit using Noll's theoretical values and the fitted  $r_0$  value. This is used as a sanity check. Note that the tip and tilt are not displayed as they are mostly meaningless when dealing with LGS data.

Fig. 2(b) shows the PSD of the differential focus for all six baselines. These are also used as a sanity check of the data. Note that, expectedly, the knee frequency is at higher frequency than the single direction focus PSD of Fig. 2(a) (5 Hz versus 1 Hz).

The noise-corrected measured differential Zernike coefficient rms structure function, i.e.  $\sigma_{\delta m_{4,5,6}}$  versus the separation  $|\theta_0|$ , is shown in Fig. 4. This plot shows results from two data sets, corresponding to an excellent seeing case (lower set of curves, from 2011 November 5) and an average seeing case (upper set, from 2012 January 8). As was already noted, there are six baselines in the GeMS constellation, indicated here by the pair of numbers above the horizontal



**Figure 2.** (a) Example of the PSD of the focus and the two astigmatism Zernike modes, and frequency cut-off for noise estimation from the high-frequency part of the spectra. The focus is shown in black, astigmatism 45 in blue and astigmatism 0 in red. (b) Example of the PSD of the differential focus for all possible baselines.



**Figure 3.** Zernike coefficient rms for all WFSs, and the fitting derived from Noll (thick red line). Example from 2012 January 8.

axis [e.g.  $\theta_0 = (\theta_x, \theta_y) = (+30, -30)$ ]. Note that to avoid crowding the plot with overlapping symbols, points corresponding to the same baseline length, but different baseline orientations, have been shifted slightly towards the left-hand or right-hand side. Angular differential rms values are shown for the focus, and the two astigmatism (see colour labels on the plot). The error bars on some of the points are equal to the rms derived from the two values available for these baselines: for example, as can be seen in Fig. 1, the value corresponding to the  $(+30, +30)$  separation can be computed from the LGS pairs [5, 1] and [1, 3]. The thin solid black line links the focus points and the dashed black line links the average of the two astigmatism. As already noted before, for the turbulent component, the focus should be equal to the astigmatism average.

<sup>2</sup> The GeMS main loop can be operated up to 800 Hz, but generally 200 or 400 Hz is used, depending on the season and laser output power.

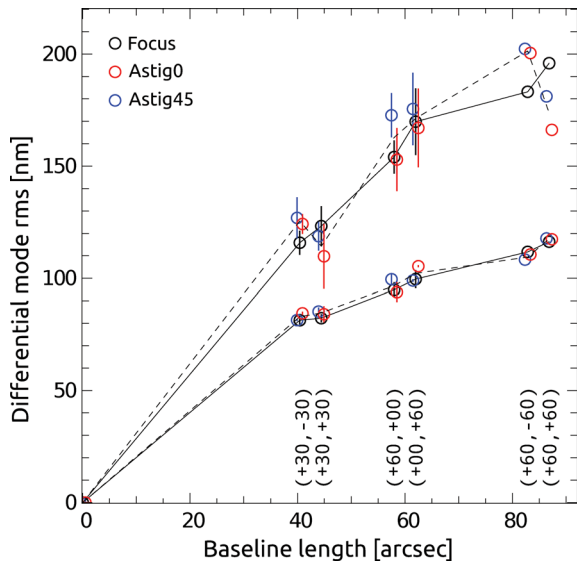


**Figure 4.** Differential focus and differential astigmatism amplitude rms versus baseline length. The top set of curves are for the night of 2012 January 8. The bottom set of curves are for 2011 November 5. See the text for a detailed explanation.

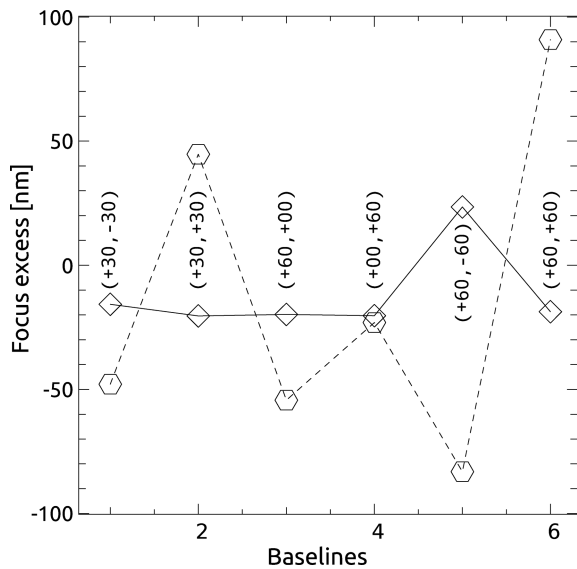


**Figure 5.** Focus excess for all possible baselines for two sample nights [baselines are reported as doublet  $(\theta_x, \theta_y)$  next to the data points]. The solid line is for the good seeing case (2011 November 5). The dashed line is for the average seeing case (2012 January 8).

This is the case for these two data sets, and indicates the absence – within the error bars – of any additional component, in particular a component that would be related to the sodium layer differential altitude between the LGSs. The good-seeing data set (bottom) provides the tightest upper limit on this differential altitude component: given that the seeing was extremely good, the differential mode rms reaches a plateau at about 100 nm. A RSS contribution from the differential altitude larger than 50 nm would certainly be seen in this data set.

Fig. 5 shows the focus excess for the two data sets shown in Fig. 4, for all six baselines. As already mentioned above, the 2011 November data show no indication of a focus excess larger than about 50 nm. The other data set was recorded in worse seeing, and

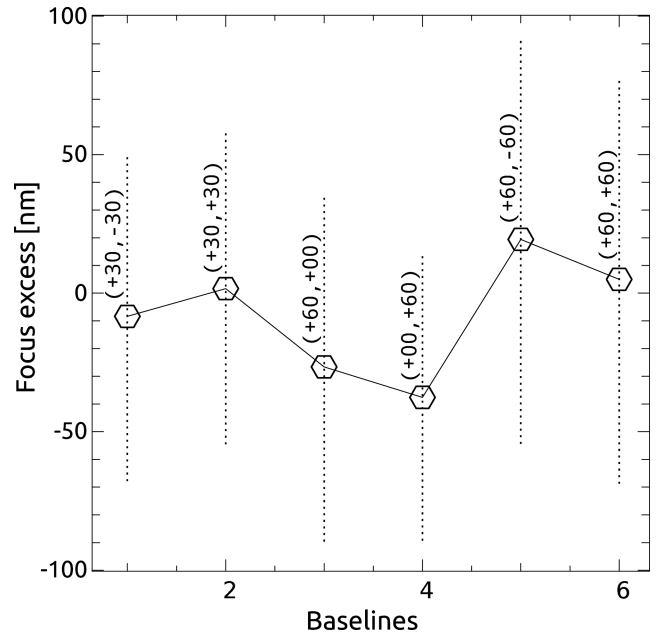


**Figure 6.** Focus excess for all possible baselines and all CBs. The solid line is the average over all CBs and the dashed error bars show the standard deviation for each baseline.

suffers from more noise. It is actually compatible with a focus excess of about 90 nm over the largest baseline  $[(60,60) \equiv 85 \text{ arcsec} \equiv 37 \text{ m at } 90 \text{ km}]$ , but this is a detection under  $1\sigma$ . Note that this data set is among those with the largest focus excess.

GeMS started on-sky commissioning in 2011 January, at a rate of five to seven nights per month. LGS WFS data have been regularly saved throughout commissioning, and 160 CBs obtained over the 2011 March to 2012 May period have been used for the current analysis. Fig. 6 extends the results of Fig. 5. For each baseline, the 160 CBs provide as many values of the focus excess, from which a mean and a rms can be computed, which are reported in Fig. 6.

Based on these results, the upper limit on the differential focus error measured by GeMS is of the order of  $15 \pm 60 \text{ nm}$  for the largest baseline of 85 arcsec (37 m at 90 km). This is compatible with the 30 nm longitudinal measurements presented in Pfrommer & Hickson (2012a), but seems to exclude the large transversal focus excess value of 280 nm found by the same authors.

As these measurements were generally done without setting the alignment of the LGS WFS to a particular value, the baselines are generally not aligned with the ‘longitudinal’ and ‘transversal’ directions; thus Fig. 6, as such, does not provide a strong constraint on the *anisotropy* detected by Pfrommer & Hickson (2012a). To further investigate a possible anisotropy in the measurements, we computed the ratio of the focus excess for all possible perpendicular baselines. This ratio is called *ellipticity* in the following. The six baselines provide three perpendicular pairs (see Fig. 1), that is, for instance,  $(+60, 0)$  with  $(0, +60)$ . This ellipticity is plotted in Fig. 7 for the 160 CBs. In this polar plot, the radius is the ellipticity value, and the angle  $\omega$  is the position angle of the pair with respect to east/west.  $\omega$  is a combination of the baseline pair offset angle, the telescope azimuth and the Cassegrain rotator position. All points are essentially distributed along a circle, with no trace of ellipticity, which indicates that, based on GeMS data, no anisotropy is detected in the

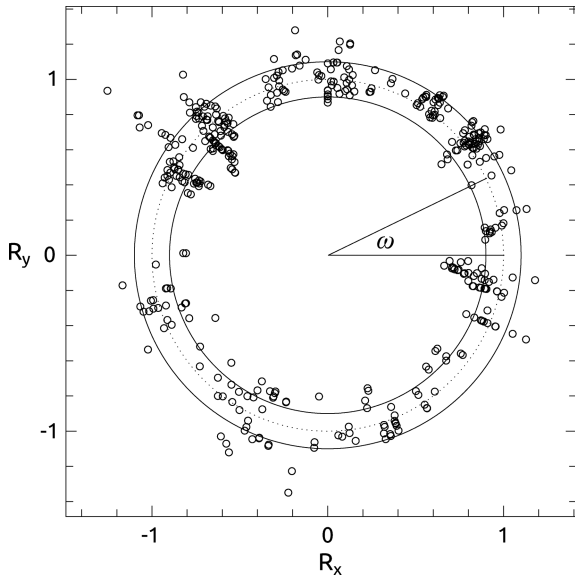


**Figure 7.** Ellipticity for all buffers (see text). The dashed circle has  $R = 1$ . The solid circles have  $R = 0.9$  and  $1.1$ .

horizontal sodium layer structure function within  $\pm 10$  per cent, in contradiction with results by Pfrommer & Hickson (2012a).

#### 4 CONCLUSION

We have presented results of the differential focus wavefront error measured from the GeMS LGS constellation. Based on data accumulated at a rate of around 1 week per month during a period of 1 year, we derive an upper limit for the differential focus error of the order of  $15 \pm 60$  nm, over a baseline of 85 arcsec and for an 8-m telescope,<sup>3</sup> or  $27 \pm 108$  m expressed in sodium layer altitude. Our data also indicate that within the relatively large error bars, the mean sodium altitude horizontal structure function is isotropic. Both these results are inconsistent with the results of Pfrommer & Hickson (2012a), which show much larger focus excess values, as well as a very strong anisotropy of this quantity. If our results were confirmed, this would have positive consequences for the ELT AO systems, which were the AO systems most affected by the findings of Pfrommer & Hickson (2012a). We intend to continue recording data from GeMS, and develop a collaboration with Pfrommer to explain the discrepancy between our results.

<sup>3</sup> To scale to another diameter, multiply by the square of the diameter ratio.

#### ACKNOWLEDGEMENTS

The Gemini Observatory is operated by the Association of Universities for Research in Astronomy, Inc., under a cooperative agreement with the NSF on behalf of the Gemini partnership: the National Science Foundation (United States), the Science and Technology Facilities Council (United Kingdom), the National Research Council (Canada), CONICYT (Chile), the Australian Research Council (Australia), Ministério da Ciência e Tecnologia (Brazil) and Ministerio de Ciencia, Tecnología e Innovación Productiva (Argentina). The authors want to acknowledge Céline Dorgeville and Rodolphe Conan for reading the manuscript and suggesting corrections and clarifications.

#### REFERENCES

- Amico P., Campbell R. D., Christou J. C., 2010, in Silva D. R., Peck A. B., Soifer B. T., eds, Proc. SPIE Vol. 7737, Observatory Operations: Strategies, Processes, and Systems III, San Diego, p. 0A-11
- d’Orgeville C. et al., 2012, in Ellebroek B. L., Marchetti E., Veran J.-P., eds, Proc. SPIE Vol. 8447, Adaptive Optics Systems III. SPIE, Amsterdam, p. 84471Q
- Foy R., Labeyrie A., 1985, *A&A*, 152, L29
- Lardiere O., Conan R., Bradley C., Jackson K., 2010, 1st AO4ELT Conference, doi: <http://dx.doi.org/10.1051/ao4elt/201005012>
- Moussaoui N., Clemesha B. R., Holzlohner R., Simonich D. M., Bonaccini Calia D., Hackenberg W., Batista P. P., 2010, *A&A*, 511, A31
- Muller N., Robert C., Michau V., Fusco T., 2010, 1st AO4ELT Conference, Anisoplanatism effects in Shack-Hartmann Wave Front Sensing with Laser Guide Stars on the ELTs, doi: <http://dx.doi.org/10.1051/ao4elt/201005015>
- Neichel B., D’Orgeville C., Callingham J., Rigaut F., Winge C., Trancho G., 2013, *MNRAS*, 429, 3522
- Noll R. J., 1976, *J. Opt. Soc. Am.*, 1976, 66, 207
- Pfrommer T., Hickson P., 2010, *J. Opt. Soc. Am. A Opt. Image Sci. Vis.*, 27, A97
- Pfrommer T., Hickson P., 2012a, in Ellebroek B. L., Marchetti E., Veran J.-P., eds, Proc. SPIE Vol. 8447, Adaptive Optics Systems III. SPIE, Amsterdam, p. 844719
- Pfrommer T., Hickson P., 2012b, in Veran J.-P., Fusco T., Clenet Y., eds, Proc. AO4ELT2, Victoria
- Pfrommer T., Hickson P., Chiao-Yao S., 2010, 1st AO4ELT Conference, doi: <http://dx.doi.org/10.1051/ao4elt/201004001>
- Rigaut F. et al., 2012, in Veran J.-P., Fusco T., Clenet Y., eds, Proc. AO4ELT2, Victoria
- Roddier F., Northcott M. J., Graves J. E., McKenna D. L., Roddier D., 1993, *J. Opt. Soc. Am. A Opt. Image Sci. Vis.*, 10, 957
- Tallon M., Foy R., 1990, *A&A*, 235, 549

This paper has been typeset from a  $\text{\TeX}/\text{\LaTeX}$  file prepared by the author.